

**Effects of nonlinear interfacial kinetics and interfacial thermal resistance in planar solidification**Benoit Palmieri,<sup>1</sup> C. A. Ward,<sup>2</sup> and Marcus Dejmek<sup>1</sup><sup>1</sup>*Canadian Space Agency, 6767 route de l'aéroport, St-Hubert, Canada, J3Y 8Y9*<sup>2</sup>*Department of Mechanical and Industrial Engineering, Thermodynamics and Kinetics Laboratory, University of Toronto, 5 King's College Road, Toronto, Canada, M5S 3G8*

(Received 7 March 2012; published 12 November 2012)

Large temperature discontinuities were recently measured at a solid-liquid interface during heat transport processes. These observations suggest that when heat flows between two phases, the interface is not well characterized by assuming thermal equilibrium. This can be of importance in rapid solidification processes. In this paper we consider a planar front model that solidifies from its undercooled melt. We use a generalized interfacial boundary condition that includes nonlinear kinetic effects and allows for a temperature discontinuity. The effects of the new boundary condition on the solidification rates and the temperature profile are reported as a function of time. Our analysis shows that the undercooling regime where constant phase-front velocities are observed at steady states (traveling-wave solutions) are unaffected by the new boundary conditions. These solutions arise when the Stephan number is larger than 1. On the other hand, the solidification rates and the steady-state velocities are greatly affected by the assumed conditions at the interface. Incorporation of an interface thermal resistance, or Kapitza resistance, generates temperature discontinuities at the interface, leads to reduced solidification rates and the Mullins-Sekerka instability arises at longer wavelengths deformation of the planar front.

DOI: [10.1103/PhysRevE.86.051605](https://doi.org/10.1103/PhysRevE.86.051605)

PACS number(s): 81.10.Fq, 64.70.D-, 05.70.Ln

**I. INTRODUCTION**

When solidification is induced in a liquid cooled below its freezing point, the solid can grow in the form of dendrites of characteristic shapes and velocities that are functions of the supercooled temperature [1,2]. The dendrites show emerging side branches that are a classical example of self-organizing microstructure formation. Dendritic growth has important industrial applications since it determines the final properties of the solid material.

The earliest theoretical models of crystal growth were due to Ivantsov [3] and Temkin [4] and neglected the buoyancy-driven convection in the melt. For a better comparison with these theories, a series of experiments called the *Isolated Dendritic Growth Experiment* (IDGE) were conducted during flights of the Space Shuttle [5–8]. For practical purposes (low melting point, transparent), pure succinonitrile (SCN) was used in many of these crystallization experiments. The theoretical models have been improved since the original work of Ivantsov and Temkin to include effects such as the flow in the melt [9,10] and surface tension anisotropy [11–13]. In these approaches and in more recent numerical crystal growth studies [14,15], the interface has been described with local equilibrium principles within each phase and thermal equilibrium across the phase boundary. This corresponds to the original description of the interface proposed by Temkin [4]: a unique interface temperature, continuous across the phase boundary, that scales linearly with the interface velocity (hereafter referred as linear kinetics).

This is an example of the standard assumption that the interfacial temperatures are equal when heat flows through the interface between a solid and a liquid. On the other hand, measurements made at liquid-He temperatures revealed temperature discontinuities [16,17]. The existence of temperature discontinuities was further supported by molecular simulations [18].

Novel steady-state evaporation studies also contradicted the linear kinetic description of the interface [19–21]. In one

particular experiment, a sessile water droplet was maintained at constant size on a Au(111) substrate by injecting water into the droplet's base at the same rate as water evaporated at its liquid-vapor interface [22]. Twelve thermocouples were embedded in the substrate and used to measure the thermal transport from the solid to the solid-liquid interface. The temperature field in the liquid phase was measured with a microthermocouple mounted on a positioning micrometer. It was found that a thermal or Kapitza resistance existed at the water-Au interface and resulted in an interfacial temperature discontinuity with the solid being as much as 2.15 K greater than that of the liquid. As a result, of the energy transported to the solid-liquid interface, only a fraction was transported *perpendicular* to this interface. A much larger portion, up to 87%, was conducted *parallel* to the solid-liquid interface, through the adsorbed layer, to the three-phase line. An energy balance showed that the thermal energy conducted through the adsorbed layer was equal to the energy distributed along the liquid-vapor interface by thermocapillary convection where it was consumed by the phase change process.

These previous studies suggest that the liquid-solid interface is not adequately characterized by assuming thermal equilibrium to exist at the solid-liquid interface. This may have important implications in solidification and crystal growth processes, especially for rapid solidification [23]. Local-equilibrium approximation is expected to break down for large rates where the system is far from equilibrium. At present, it is unclear what assumptions should be made in describing the interface during solidification. Using a planar solidification model, we consider three possibilities: (1) temperature equality and linear kinetics, (2) a nonlinear kinetics relation obtained from statistical rate theory [24–27] and temperature equality, and (3) nonlinear kinetics and temperature discontinuity. The nonlinear kinetics employed allows for a temperature discontinuity and does not contain any new fitting parameters. An important difference between this system and the experimental evaporation studies described

above is that the position of the solid surface moves as the phase change process occurs.

Planar front solidification has been extensively studied with boundary conditions at the interface that assumes local equilibrium in each phase and thermal equilibrium across the interface [28,29]. Also, the role of temperature discontinuities in the planar front model has been studied before us. In the approach used by Fried and Shen [30], a linear kinetic relation was used and steady state was assumed from the onset. Also, the work of Galenko *et al.* [31] included a finite speed for the heat transfer that gives rise to a hyperbolic equation rather than a simple diffusion equation for the evolution of the temperature profile. The purpose of this work is to use a fully nonlinear kinetic description of the interface that allows for a temperature discontinuity and to report its effect on the dynamics and the temperature profile of an initially supercooled system where a planar front separates a solid and a liquid phase. Combining numerical and analytical techniques, the state of the system can be reported at all times.

The paper is divided as follows. Section II reports the equations governing the system and sets the stage for the interfacial boundary conditions described in Sec. III. Section IV contains our results. In Sec. IV A we first give details on our numerical and analytical procedure and report the effect of the nonlinear kinetics on the planar front velocity and on the full temperature profile at short, intermediate, and long times for a system with zero Kapitza resistance. We then generalize to the case of a nonzero Kapitza resistance in Sec. IV B and report its effects on the Mullins-Sekerka instability. Section V is the discussion and contains concluding remarks; Appendices A and B give more details on the analytic and numerical methods used.

## II. PROBLEM DEFINITION

The governing equations are

$$\frac{\partial T_S(x,t)}{\partial t} = D_S \frac{\partial^2 T_S(x,t)}{\partial x^2}, \quad 0 < x < X_I(t), \quad (2.1)$$

$$\frac{\partial T_L(x,t)}{\partial t} = D_L \frac{\partial^2 T_L(x,t)}{\partial x^2}, \quad X_I(t) < x < \infty, \quad (2.2)$$

where  $T_{S(L)}$  and  $D_{S(L)}$  are, respectively, the temperature and the thermal diffusivities in the solid (liquid) phase and  $X_I(t)$  is the position of the interface at time  $t$ . Boundary conditions are imposed at the interface and at the system's boundaries ( $x = 0$  and  $x = \infty$ ). We consider a semi-infinite system in contact with a heat bath at  $x = \infty$  and isolated at  $x = 0$ . Therefore,

$$\left( \frac{\partial T_S(x,t)}{\partial x} \right)_{x=0} = 0, \quad (2.3)$$

$$T_L(x = \infty, t) = T_{\text{Bulk}}, \quad (2.4)$$

where  $T_{\text{Bulk}}$  is the temperature far from the interface. It is also denoted as the ‘‘supercooled’’ temperature. Initially, the system's temperature is uniform and equal to  $T_{\text{Bulk}}$  in both phases and the interface position is equal to  $\epsilon$ :

$$T_{S(L)}(x, t = 0) = T_{\text{Bulk}}, \quad (2.5)$$

$$X_I(t = 0) = \epsilon. \quad (2.6)$$

When solidification occurs, latent heat is released as the interface advances and conservation of energy imposes the following boundary condition at the interface,

$$\rho_S \dot{X}_I(t) \lambda = \rho_S C_S D_S \left( \frac{\partial T_S(x,t)}{\partial x} \right)_{x=X_I(t)} - \rho_L C_L D_L \left( \frac{\partial T_L(x,t)}{\partial x} \right)_{x=X_I(t)}, \quad (2.7)$$

where  $\lambda$  is the latent heat and  $\rho_{S(L)}$  and  $C_{S(L)}$  are, respectively, the density and the heat capacity of the solid (liquid). The interface velocity is the time derivative of the interface position and is denoted by  $\dot{X}_I(t)$ .

The problem is fully specified when a further boundary condition fixes the interface temperature. For a temperature profile that is continuous across the interface, we write it as

$$T_S(x = X_I(t), t) = T_L(x = X_I(t), t) = T_I(\dot{X}_I(t)). \quad (2.8)$$

At equilibrium, the temperature is uniform and equal to the melting temperature ( $T_I = T_{\text{Melt}}$ ) and  $\dot{X}_I(t) = 0$ . Hence, one of the boundary condition that was used in previous work was [32],

$$T_I(\dot{X}_I(t)) = T_{\text{Melt}}. \quad (2.9)$$

This boundary condition assumes local equilibrium in the interface region. The system is initially supercooled so that  $T_{\text{Bulk}} < T_{\text{Melt}}$ . The problem is exactly solvable with such a boundary condition, and it results in an interface motion that scales as  $X_I(t) \propto t^{1/2}$ . Therefore, the interface velocity scales like  $\dot{X}_I(t) \propto t^{-1/2}$  and vanishes at long times. No traveling-wave solutions (i.e., steady-state solutions with a nonzero interface velocity) are found. With such an interfacial boundary condition, the system tends toward equilibrium at infinitely long times.

Nonzero steady-state velocity solutions can be obtained when interfacial kinetics is introduced into the problem [28,29]. In this case the interface temperature is related to the interface velocity,

$$T_I(\dot{X}_I(t)) = T_{\text{Melt}} - a \dot{X}_I(t), \quad (2.10)$$

where  $a$  is called the molecular attachment coefficient. Energy conservation arguments show that traveling-wave solutions are obtained when  $\text{St} > 1$  where the Stefan number is a dimensionless parameter defined as  $\text{St} = C_L(T_{\text{Melt}} - T_{\text{Bulk}})/\lambda$ . Hence, when the supercooling is large enough, equilibrium is never reached even at infinitely long time.

Our goal is to generalize the interfacial boundary conditions to include nonlinear kinetics and nonzero Kapitza resistance and study their effects on the solidification process numerically and analytically.

## III. INTERFACIAL BOUNDARY CONDITIONS

The following dimensionless units are introduced:

$$\tilde{T} = T/T_{\text{Melt}}, \quad \tilde{x} = x/\epsilon, \quad \tilde{t} = tD/\epsilon^2, \quad (3.1)$$

and the above-mentioned governing equations can then be rewritten in dimensionless units:

$$\frac{\partial \tilde{T}_S(\tilde{x}, \tilde{t})}{\partial \tilde{t}} = \frac{\partial^2 \tilde{T}_S(\tilde{x}, \tilde{t})}{\partial \tilde{x}^2}, \quad 0 < \tilde{x} < \tilde{X}_I(\tilde{t}), \quad (3.2a)$$

$$\frac{\partial \tilde{T}_L(\tilde{x}, \tilde{t})}{\partial \tilde{t}} = \frac{\partial^2 \tilde{T}_L(\tilde{x}, \tilde{t})}{\partial \tilde{x}^2}, \quad \tilde{X}_I(\tilde{t}) < \tilde{x} < \infty, \quad (3.2b)$$

$$\left( \frac{\partial \tilde{T}_S(\tilde{x}, \tilde{t})}{\partial \tilde{x}} \right)_{\tilde{x}=0} = 0, \quad (3.2c)$$

$$\tilde{T}_L(\tilde{x} = \infty, \tilde{t}) = \tilde{T}_{\text{Bulk}}, \quad (3.2d)$$

$$\tilde{T}_{S(L)}(\tilde{x}, \tilde{t} = 0) = \tilde{T}_{\text{Bulk}}, \quad (3.2e)$$

$$\tilde{X}_I(\tilde{t} = 0) = 1. \quad (3.2f)$$

In this work we consider the simplest system possible and focus on interfacial effects only. Hence, we set  $C_S = C_L = C$ ,  $\rho_S = \rho_L = \rho$ , and  $D_S = D_L = D$  for simplicity. These dimensionless units will be used for the remainder of the paper, unless otherwise specified.

### A. Interfacial thermal resistance

As discussed in Ref. [17], nonzero interface resistivities lead to temperature jumps in the interface region when there is a nonvanishing heat flux across the interface. This statement can be recast as

$$\tilde{J}_Q = -\tilde{R}_I^{-1}(\tilde{T}_L(\tilde{X}_I(\tilde{t}), \tilde{t}) - \tilde{T}_S(\tilde{X}_I(\tilde{t}), \tilde{t})), \quad (3.3)$$

where  $\tilde{J}_Q$  is the heat flux through the interface and  $\tilde{R}_I$  is the interfacial resistivity or Kapitza resistance.

Provided that we have an expression for the heat flux, an interfacial resistivity can be introduced in the model. Because many recent experiments reported significant temperature jumps [19,22,33], one of our goals is to show how the planar front behavior is modified when the interfacial resistivity deviates from zero.

We first need an expression for the heat flux through the interface. We derive it directly from the first law of thermodynamics using the above simplifications for the material properties. As solidification takes place, there is no expansion or pressure change and therefore, no work is done by the system. In analogy with the first law, the heat flux is equal to the energy flux through the interface,  $\tilde{J}_E(t)$ :

$$\tilde{J}_Q(t) = \tilde{J}_E(t). \quad (3.4)$$

Because the boundary is moving, one can show that the total amount of energy that crosses the boundary in a small time period  $\delta t$  is  $-\rho \dot{X}_I(t) E_L(T_L(X_I(t), t)) A \delta t$  where  $E_L$  is the internal energy in the liquid phase at the appropriate temperature and  $A$  is the area of the plane. For clarity, the total amount of energy that crosses the boundary was

$$\rho_s \dot{X}_I(t) = K_{\text{eq}} \sinh \left[ \frac{H_L(T_L(X_I(t), t), P_L) - H_S(T_S(X_I(t), t), P_S)}{k_B \Theta} + \frac{S_S(T_S(X_I(t), t), P_S) - S_L(T_L(X_I(t), t), P_L)}{k_B} \right], \quad (3.9)$$

where  $H_{S(L)}$  and  $S_{S(L)}$  are the enthalpies and the entropies of the solid (liquid) phase,  $P_{S(L)}$  is the pressure of the solid (liquid) phase  $k_B$  is Boltzmann's constant,  $K_{\text{eq}}$  is the unidirectional equilibrium rate constant, and

$$\Theta \equiv \frac{C_S T_S + C_L T_L}{C_S + C_L}$$

written with its appropriate units. Heat is released as the interface is moving and part of this energy comes back to the liquid phase diffusively. This contributes an amount equal to  $-\rho C D (\partial T_L(x, t) / \partial x)_{x=X_I(t)} A \delta t$ . Hence, in dimensionless units the heat flux becomes

$$\begin{aligned} \tilde{J}_Q(t) &= -\dot{\tilde{X}}_I(\tilde{t}) \tilde{E}_L(\tilde{T}_L(\tilde{X}_I(\tilde{t}), \tilde{t})) - \left( \frac{\partial \tilde{T}_L(\tilde{x}, \tilde{t})}{\partial \tilde{x}} \right)_{\tilde{x}=\tilde{X}_I(\tilde{t})} \\ &= -\dot{\tilde{X}}_I(\tilde{t}) \tilde{E}_S(\tilde{T}_S(\tilde{X}_I(\tilde{t}), \tilde{t})) - \left( \frac{\partial \tilde{T}_S(\tilde{x}, \tilde{t})}{\partial \tilde{x}} \right)_{\tilde{x}=\tilde{X}_I(\tilde{t})}, \end{aligned} \quad (3.5)$$

where  $\tilde{E} = E/CT_{\text{Melt}}$  and

$$\tilde{E}_s = \tilde{T}_s, \quad \tilde{E}_L = \tilde{T}_L + \alpha, \quad (3.6)$$

and where we introduced a new dimensionless variable:

$$\alpha = \lambda / (CT_{\text{Melt}}). \quad (3.7)$$

The second line in Eq. (3.5) is derived similarly, but considering the energy flow from the solid phase. We then demand that the two expressions be equal and obtain a Stephan-like boundary condition. This is a modified version of Eq. (2.7) for energy conservation that accounts for a temperature jump at the interface:

$$\begin{aligned} &\dot{\tilde{X}}_I(\tilde{t}) (\alpha + \tilde{T}_L(\tilde{X}_I(\tilde{t}), \tilde{t}) - \tilde{T}_S(\tilde{X}_I(\tilde{t}), \tilde{t})) \\ &= \left( \frac{\partial \tilde{T}_S(\tilde{x}, \tilde{t})}{\partial \tilde{x}} \right)_{\tilde{x}=\tilde{X}_I(\tilde{t})} - \left( \frac{\partial \tilde{T}_L(\tilde{x}, \tilde{t})}{\partial \tilde{x}} \right)_{\tilde{x}=\tilde{X}_I(\tilde{t})}. \end{aligned} \quad (3.8)$$

Note that our expression for the heat flux differs from that of Fried *et al.* [30] where the heat flux through the interface is defined in terms of an entropy flux instead of an internal energy flux. Their relation is derived by analogy with the second law of thermodynamics. Hence, we believe that their relation gives an upper bound for the heat flux, which will be valid for any kind of solidification process. Our expression is less general, but is nevertheless exact for our simplified model system where no work is done.

### B. Nonlinear interfacial kinetics

Statistical Rate theory gives an expression for the rate of phase change as a function of the thermodynamic properties of both phases in regions infinitesimally close to the interface [27,34,35]. The expression resulting from SRT has been tested experimentally in numerous evaporation experiments, but it can be generally applied to any kind of phase change. In the context of planar solidification, it can be written with real units as follows:

is the equilibrium temperature of two phases initially at  $T_S$  and  $T_L$  when only heat exchanges are allowed between them. Note that this expression allows for a temperature discontinuity at the interface. It reduces to Eq. (2.10) close to equilibrium (when the argument in the sinh is small) and when the two interfacial temperatures are equal. For more details on the

development of SRT and its use in recent experiments, see the appropriate literature [27,36–38].

Equation (3.9) can be used as is. For many materials, the temperature and pressure dependence of the enthalpies and entropies are well known [39]. Here, we simply expand them about  $T = T_{\text{Melt}}$ . With these simplifications and written in dimensionless units, the following expression is obtained,

$$\begin{aligned} \dot{X}_I(\tilde{t}) = \beta \sinh \left( \gamma \left\{ \frac{2}{\tilde{T}_S^I + \tilde{T}_L^I} - 1 \right. \right. \\ \left. \left. + \alpha^{-1} \left[ \frac{2(\tilde{T}_L^I - \tilde{T}_S^I)}{\tilde{T}_S^I + \tilde{T}_L^I} - \ln \frac{\tilde{T}_L^I}{\tilde{T}_S^I} \right] \right\} \right) = \tilde{J}_N(\tilde{t}), \end{aligned} \quad (3.10)$$

where we introduced two more dimensionless variables,

$$\gamma = \lambda / (k_B T_{\text{Melt}}), \quad \beta = K_{\text{eq}} \epsilon / (\rho D), \quad (3.11)$$

and where  $\tilde{J}_N(\tilde{t})$  is the net dimensionless flux of molecules undergoing phase change. When the interface temperatures are the same and equal  $\tilde{T}_I$ , this equation reduces to

$$\dot{X}_I(\tilde{t}) = \beta \sinh \left( \gamma \left[ \frac{1}{\tilde{T}_I} - 1 \right] \right). \quad (3.12)$$

If  $\tilde{T}_I$  is close and below 1, it reduces to Eq. (2.10) with  $a^{-1} = \beta\gamma$ . Equation (3.10) goes beyond the regime of validity of Eq. (2.10). It should allow us to describe rapid solidification processes, when the initial state of the system is far from equilibrium. Note that  $\dot{X}_I(\tilde{t}) = 0$  when  $\tilde{T}_S^I = \tilde{T}_L^I = 1$ , as expected.

As a final comments, we show how Eqs. (3.10) and (3.3) obey the Onsager reciprocal relations [40]. These relationships hold in the linear regime, so we proceed by writing  $\tilde{T}_S^I = 1 - \tilde{\Delta}_S^I$  and  $\tilde{T}_L^I = 1 - \tilde{\Delta}_L^I$  in Eq. (3.10) and expand the result to first order in  $\tilde{\Delta}_L^I$  to obtain the following expression:

$$\begin{aligned} \tilde{J}_N(\tilde{t}) &\approx \beta\gamma \left( \frac{\tilde{\Delta}_L^I + \tilde{\Delta}_S^I}{2} \right) + O(\tilde{\Delta}_{L,S}^I)^2 \\ &= \beta\gamma \left( 1 - \frac{\tilde{T}_L^I + \tilde{T}_S^I}{2} \right) + O(\tilde{\Delta}_{L,S}^I)^2. \end{aligned} \quad (3.13)$$

Note that  $1 - (\tilde{T}_L^I + \tilde{T}_S^I)/2 = \alpha C T_{\text{Melt}} [\mu_L(\Theta) - \mu_S(\Theta)]$  in the linear regime where  $\mu_{L/S}$  is the chemical potential in the liquid or solid phase and where  $\Theta = (\tilde{T}_L^I + \tilde{T}_S^I)/2$  is the mean temperature in the two phases. In the linear regime, Eq. (3.10) does not contain any term proportional to the interfacial temperature discontinuity. The Onsager relations therefore require that Eq. (3.3) does not contain any term proportional to the mean interfacial temperature or the chemical potential difference. This restriction is satisfied because Eq. (3.3) is linear in the temperature difference only. Cross-effects in the expressions for  $\tilde{J}_N$  and  $\tilde{J}_Q$  do not appear in the linear regime of the model used. These have been studied by others in the context of the crystallization of helium crystals [41]. We do not include them here because one of our goals is to apply the nonlinear interfacial kinetic expression provided by SRT to planar solidification, a theory that does not contain any cross terms in the linear regime. Also note that, for a particular osmotic transport example, it was previously

demonstrated how SRT is consistent with the Onsager reciprocal relations [42].

We now show how the solidification process is modified when SRT replaces the linear interfacial kinetics boundary condition with and without a Kapitza resistance.

## IV. RESULTS

### A. No interfacial thermal resistance: $\tilde{R}_I = 0$

#### 1. Long-time asymptotics

The problem cannot be solved exactly but analytical predictions for the long-time behavior of the planar front can be obtained using a procedure developed by Charach *et al.* [28]. Some details on Charach's procedure are given in Appendix A. Here we simply state the main results.

At long-time, the temperature profile in the solid becomes a constant, and the one in the liquid depends on the Stephan number. Modifications of Charach's results when a nonlinear interfacial kinetics [Eq. (3.12)] is incorporated are now summarized.

For  $\text{St} < 1$ , we are in the so-called diffusion limited regime, the long-time temperature profiles are

$$\begin{aligned} \tilde{T}_S(\tilde{x}, \tilde{t}) &= 1 + O(\tilde{t}^{-1/2}), \\ \tilde{T}_L(\tilde{x}, \tilde{t}) &= \tilde{T}_{\text{Bulk}} + \frac{1 - \tilde{T}_{\text{Bulk}}}{\text{erfc}(c/2)} \text{erfc}(\tilde{x}/2\tilde{t}^{1/2}) + O(\tilde{t}^{-1/2}), \end{aligned} \quad (4.1)$$

in dimensionless units. There,  $\text{erfc}$  is the complimentary error function, and the constant  $c$  is related to the Stephan number as follows:

$$\text{St} = \pi^{1/2} \frac{c}{2} e^{c^2/4} \text{erfc}(c/2). \quad (4.2)$$

In this regime the long-time dynamics of the interface is given by  $\dot{X}_I(\tilde{t}) = c\tilde{t}^{1/2}$  and  $\dot{X}_I(\tilde{t}) = c\tilde{t}^{-1/2}/2$ . No traveling-wave solutions are found for  $\text{St} < 1$ , irrespective of the relationship between growth velocity and interfacial temperature.

For  $\text{St} > 1$ , called the interfacial kinetics limited regime,

$$\begin{aligned} \tilde{T}_S(\tilde{x}, \tilde{t}) &= \tilde{T}_I^{ss} + O(\tilde{t}^{-1}), \\ \tilde{T}_L(\tilde{x}, \tilde{t}) &= \tilde{T}_{\text{Bulk}} + (\tilde{T}_I^{ss} - \tilde{T}_{\text{Bulk}}) e^{-\tilde{V}^{ss}(\tilde{x} - \tilde{V}^{ss}\tilde{t})} \\ &\quad + \text{exponentially small corrections}, \end{aligned} \quad (4.3)$$

where

$$\tilde{T}_I^{ss} = \alpha + \tilde{T}_{\text{Bulk}} \quad (4.4)$$

and  $\tilde{V}^{ss}$  are, respectively, the steady-state interface temperature and interface velocity. They are nonlinearly related through

$$\tilde{T}_I^{ss} = F(\tilde{V}^{ss}) \equiv \frac{\gamma}{\gamma + \text{arcsinh}(\tilde{V}^{ss}/\beta)}. \quad (4.5)$$

In this regime, traveling-wave solutions are obtained. At long times,  $\dot{X}_I(\tilde{t}) = \tilde{V}^{ss}\tilde{t}$  and  $\dot{X}_I(\tilde{t}) = \tilde{V}^{ss}$ . Nonlinearities in the interfacial kinetics change the steady-state velocity. For all supercooling, the interface temperature at long time is unaffected by the nonlinearities in the interfacial kinetic. It is either  $\tilde{T}_I^{ss} = \tilde{T}_{\text{Melt}}$  ( $\text{St} < 1$ ) or  $\tilde{T}_I^{ss} = \alpha + \tilde{T}_{\text{Bulk}}$  ( $\text{St} > 1$ ).

The case  $\text{St} = 1$  is special and well documented in the literature [28,43,44]. In this case, heat diffusion and interfacial

kinetics play an equally important role in the solidification process. The position and velocity of the interface scales like  $\tilde{X}_I(\tilde{t}) \propto \tilde{t}^{2/3}$  and  $\dot{\tilde{X}}_I(\tilde{t}) \propto \tilde{t}^{-1/3}$ , also irrespective of the relationship between growth velocity and interfacial temperature.

## 2. Numerical analysis

The numerical propagation of the phase front is more easily performed when the governing equations of the system are written as

$$\frac{\partial \tilde{T}}{\partial \tilde{t}} = \frac{\partial^2 \tilde{T}}{\partial \tilde{x}^2} + \alpha \dot{\tilde{X}}_I(\tilde{t}) [\delta(\tilde{x} - \tilde{X}_I(\tilde{t})) + \delta(\tilde{x} + \tilde{X}_I(\tilde{t}))],$$

$$-\infty < \tilde{x} < \infty. \quad (4.6)$$

Instead of using a diffusion equation for each phase and imposing the Stephan condition at the interface [Eq. (2.7)], we use a single diffusion equation for both phases, but we introduce a source describing the heat released as the front is moving. Note that the latent heat enters the definition of the parameter  $\alpha$ , which depends only on material properties. The resulting temperature profile is guaranteed to satisfy the Stephan boundary condition, Eq. (2.7). The zero heat flux boundary condition at  $\tilde{x} = 0$  is satisfied by introducing a mirror image source that propagates along the negative  $\tilde{x}$  axis and imposing  $\tilde{T}_I(\tilde{x} = \pm\infty, \tilde{t}) = \tilde{T}_{\text{Bulk}}$ . In dimensionless units,  $\tilde{X}_I(0) = 1$  and  $\tilde{T}(\tilde{x}, 0) = \tilde{T}_{\text{Bulk}}$ .

The solution to Eq. (4.6) can be easily obtained with Fourier transform techniques and gives

$$\tilde{T}(\tilde{x}, \tilde{t}) = \tilde{T}_{\text{Bulk}} + \alpha \int_0^{\tilde{t}} d\tilde{\tau} \frac{e^{-[\tilde{x} - \tilde{X}_I(\tilde{\tau})]^2/4(\tilde{t} - \tilde{\tau})} + e^{-[\tilde{x} + \tilde{X}_I(\tilde{\tau})]^2/4(\tilde{t} - \tilde{\tau})}}{[4\pi(\tilde{t} - \tilde{\tau})]^{1/2}} \dot{\tilde{X}}_I(\tilde{\tau}), \quad (4.7)$$

a solution similar to the one explained in Sec. 11.4 of Ref. [32] with different boundary conditions. Combined with the nonlinear interfacial boundary condition,

$$\dot{\tilde{X}}_I(\tilde{t}) = \beta \sinh \left[ \gamma \left( \frac{1}{\tilde{T}_I} - 1 \right) \right], \quad (4.8)$$

where  $\tilde{T}_I = \tilde{T}(\tilde{x} = \pm\tilde{X}_I(\tilde{t}), \tilde{t})$ , the complete solution for the temperature profile and the phase-front position at all times can be obtained numerically. This is done using an iterative procedure based on the discrete form of the integral appearing in Eq. (4.7) and described in Appendix B.

Figure 1 shows the dimensionless phase-front velocity and temperature as a function of time for five different supercooling scenarios. The materials parameters that we used to obtain  $\alpha$  and  $\gamma$  are the ones of succinonitrile and can be found in Ref. [45]. The velocities are reported as

$\dot{\tilde{X}}_I(\tilde{t})/\beta$ . In dimensionless units, the Stephan number can be written as  $\text{St} = (1 - \tilde{T}_{\text{Bulk}})/\alpha$ . The cases shown are  $\text{St} = 0.5, 1.0, 3.0, 6.1, 10.0$ . As shown previously,  $\text{St}$  is the parameter that determines the long-time behavior of the phase front. The figures show many noticeable effects of the nonlinear interfacial kinetics. When  $\text{St} > 1$ , the long-time steady-state velocity is increased when nonlinear kinetics is introduced. Also, the time scale at which the system evolves is much faster when nonlinearities are included. For SCN, when  $\text{St} < 1$ , the two cases are almost identical. This may not be true for other materials. On the other hand, in that supercooling range, linear or nonlinear interfacial kinetics will always lead to equilibrium behavior at long times [ $\dot{\tilde{X}}_I(\tilde{t})/\beta \rightarrow 0$  and  $\tilde{T}_{\text{Bulk}} \rightarrow 1$ ]. The final steady-state temperature is not affected by the nonlinearities in the interfacial kinetics for any  $\text{St}$ . As shown in Fig. 1, the long-time asymptotic prediction is

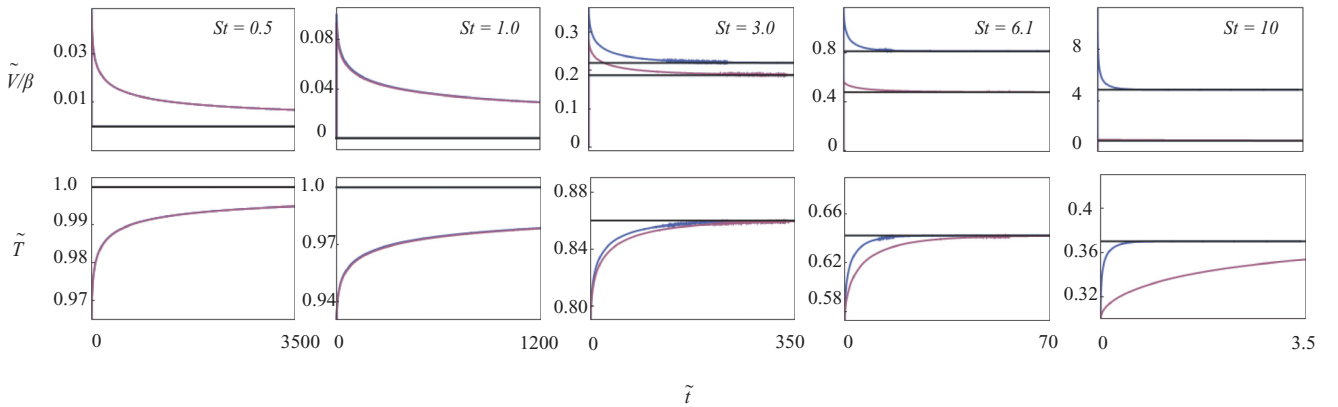


FIG. 1. (Color online) The dimensionless velocity  $[\dot{\tilde{X}}_I(\tilde{t})/\beta]$  (top panels) and the dimensionless temperature (bottom panels) of the phase front are shown as a function of dimensionless time when the interfacial kinetics is described by SRT [Eq. (4.8)] (blue, top curve) or by the linear kinetics relation (magenta, bottom curve). From left to the right, the initial dimensionless temperature is  $\tilde{T}_{\text{Bulk}} = 0.965, 0.93, 0.79, 0.572645, 0.3$ . We used succinonitrile's material dimensionless parameter ( $\alpha = 0.07$  and  $\gamma = 1.34$ ). Accordingly, the Stephan number is  $\text{St} = 0.5, 1.0, 3, 6.1, 10$ . The noisy parts of the curves are due to errors associated with the numerical scheme. The straight black lines are the long-time steady-state predictions described in Sec. IV A1. Note the faster dynamics that results from the nonlinear interfacial kinetics.

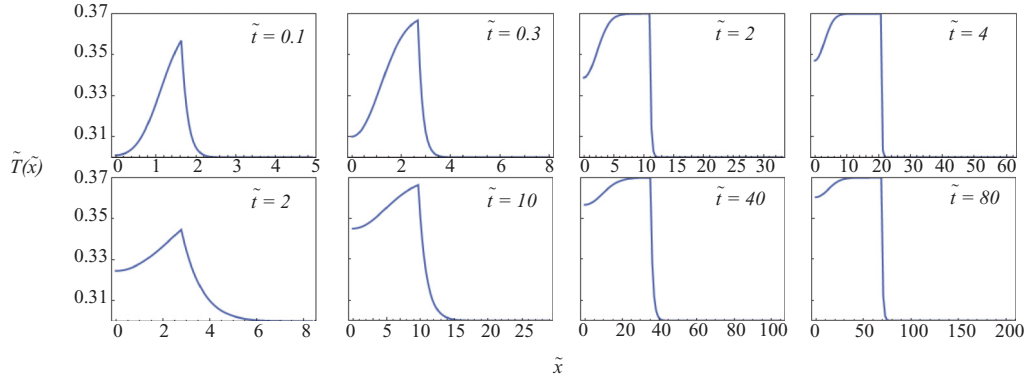


FIG. 2. (Color online) The temperature profile for  $\tilde{T}_{\text{Bulk}} = 0.3$  (both  $\tilde{T}$  and  $\tilde{x}$  are dimensionless). Top row, from left to right, the temperature profile is shown for four different increasing times:  $\tilde{t} = 0.1, 0.3, 2,$  and  $4$ . SRT provides the nonlinear interfacial kinetic boundary condition. Bottom row, the temperature profile is shown for four different increasing times:  $\tilde{t} = 2, 10, 40,$  and  $80$ . The interfacial kinetic boundary is linearized. In both rows, as the panel goes to the right, steady state is approached.

in excellent agreement with the numerical solution for all supercoolings.

In Figs. 2 and 4 the temperature profile for the supercooling  $\tilde{T}_{\text{Bulk}} = 0.3$  and  $0.965$  are shown for four different values of  $\tilde{t}$ . There, the temperature profile that results from nonlinear and linear interfacial kinetic boundary conditions are compared.

Clearly, Fig. 2 shows how the time scales at which the system evolves is drastically shortened when the nonlinear boundary condition is used at large supercooling. Hence, steady state is attained much faster.

Interestingly, Fig. 2 shows that the system has a whole did not reach steady state, even when  $\tilde{t} = 4$  (or  $80$  for the linear case). Indeed, the interface advances with a steady-state velocity well before that time, as shown in Fig. 1, but close to the  $\tilde{x} = 0$  boundary, the system is still evolving nonsteadily. This is explained because the interface moves very quickly away from that boundary and the interface is unable to provide any heat to that region of the system after a very short amount of time. Hence, for small  $\tilde{T}_{\text{Bulk}}$ , heat diffusion quickly becomes the only mechanism that increases the temperature close to  $\tilde{x} = 0$ . This diffusion process is slow compared to the solidification dynamics. In Fig. 3 the temperature at  $\tilde{x} = 0$  is reported as a function of time. Its value slowly tends to the interfacial

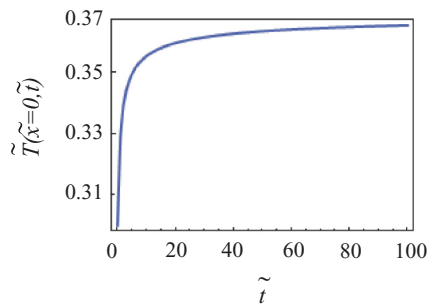


FIG. 3. (Color online) The temperature at the boundary in the solid ( $\tilde{x} = 0$ ) is displayed as a function of time  $\tilde{t}$  ( $\tilde{T}$  and  $\tilde{t}$  are in dimensionless units) for the case where  $\tilde{T}_{\text{Bulk}} = 0.3$  (largest supercooling). At long times, it tends towards the interfacial steady-state value,  $\tilde{T}_{\text{Bulk}} + \alpha = 0.37$  in this case.

steady-state temperature at long times. In fact, Fig. 3 shows that even at  $\tilde{t} = 100$ ,  $\tilde{T}(\tilde{x} = 0, \tilde{t})$  did not quite reach its steady-state value of  $0.37$ , while at the interface, that temperature is attained well within  $\tilde{t} = 3.5$  as shown in Fig. 1.

On the other hand, Fig. 4 shows that the nonlinearities in the interfacial kinetics do not play any role for small  $St$  values. The two curves shown in the figure represent the simulated temperature profiles with linear and nonlinear interfacial kinetics and they overlap. For such a small supercooling, the time evolution of the system is dominated by heat diffusion and is much slower. The figure shows that the interface temperature tends to  $1$  and the temperature profile in the solid flattens out. On the other hand, for all times shown in Fig. 4, nonzero temperature gradients in the solid are observed. Also note that the temperature in the liquid decreases to  $\tilde{T}_{\text{Bulk}} = 0.965$  at  $\tilde{x} \rightarrow \infty$ , but very smoothly compared to what is shown in Fig. 2.

In Fig. 5 the steady-state velocity as predicted by the long-time asymptotic analysis is shown as a function of  $\tilde{T}_{\text{Bulk}}$  using SCN materials properties. The relationship between the steady-state velocity and the supercooled temperature is compared for the cases of linear or nonlinear interfacial kinetics. The points on the figure corresponds to the cases studied numerically. Recall that, for SCN, when  $0.93 < \tilde{T}_{\text{Bulk}} < 1$ ,  $\tilde{V}_{ss} = 0$  (i.e.,  $St < 1$ ).

## B. Finite interfacial thermal resistance: $\tilde{R}_l \neq 0$

We repeat the methodology presented in the previous subsection, but we incorporate a nonzero thermal resistance.

### 1. Long-time asymptotics

The analysis of Charach *et al.* is repeated with a nonzero interfacial thermal resistance. The details are described in Appendix A. Again, the solutions at long times depends on the initial supercooling described by the Stephan number of the system.

For  $St < 1$ , there is are no temperature jumps at long times. Hence, the long-time temperature profile remains unchanged and is given in Sec. IV A1.

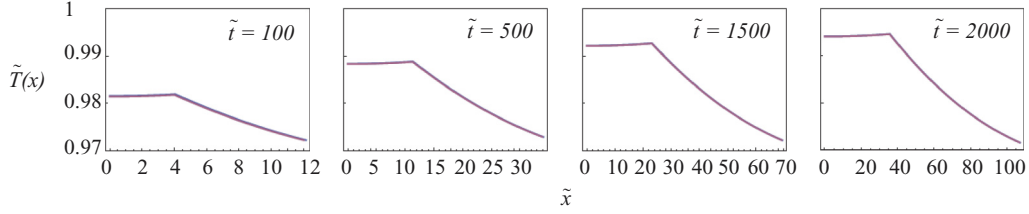


FIG. 4. (Color online) The temperature profile for  $\tilde{T}_{\text{Bulk}} = 0.965$  (both  $\tilde{T}$  and  $\tilde{x}$  are dimensionless). From left to right, the temperature profile is shown for four different increasing times:  $\tilde{t} = 100, 500, 1500$ , and  $3000$ . For the magenta (blue) curve, nonlinear (linear) interfacial kinetic boundary condition is used. The two curves are hardly distinguishable. In this regime the interface boundary condition has little effect on the temperature profile. From left to right, steady state is approached.

For  $St > 1$ , the temperature jumps survives at long times. Traveling-wave solutions are again obtained, and the temperature profiles in both phases are

$$\begin{aligned} \tilde{T}_S(\tilde{x}, \tilde{t}) &= \tilde{T}_S^I, \\ \tilde{T}_L(\tilde{x}, \tilde{t}) &= \tilde{T}_{\text{Bulk}} + (\tilde{T}_L^I - \tilde{T}_{\text{Bulk}})e^{-\tilde{V}_{ss}(\tilde{x} - \tilde{V}_{ss}\tilde{t})} \\ &\quad + \text{exponentially small corrections,} \end{aligned} \quad (4.9)$$

where

$$\tilde{T}_S^I = \alpha + \tilde{T}_{\text{Bulk}}, \quad \tilde{T}_L^I = (1 + \tilde{R}_I \tilde{V}_{SS})\tilde{T}_S^I, \quad (4.10)$$

and the steady-state velocity is obtained by solving

$$\begin{aligned} \frac{\tilde{V}_{SS}}{\beta} &= \sinh \left( \gamma \left\{ \frac{2}{\tilde{T}_S^I + \tilde{T}_L^I} - 1 \right. \right. \\ &\quad \left. \left. + \alpha^{-1} \left[ \frac{2(\tilde{T}_L^I - \tilde{T}_S^I)}{\tilde{T}_S^I + \tilde{T}_L^I} - \ln \frac{\tilde{T}_L^I}{\tilde{T}_S^I} \right] \right\} \right), \end{aligned} \quad (4.11)$$

remembering that  $\tilde{T}_L^I$  depends on  $\tilde{V}_{SS}$ . One can show that for any positive  $\tilde{R}_I$ , the resulting steady-state velocity is smaller than the one obtained when  $\tilde{R}_I = 0$ . As expected, a finite thermal resistance slows down the solidification dynamics.

## 2. Numerical analysis

When an interfacial thermal resistivity is introduced, the propagation of the temperature profile is obtained solving

$$\begin{aligned} \frac{\partial \tilde{T}}{\partial \tilde{t}} &= \frac{\partial^2 \tilde{T}}{\partial \tilde{x}^2} + \alpha \dot{\tilde{X}}_I(\tilde{t}) \{ \delta[\tilde{x} - \tilde{X}_I(\tilde{t})] + \delta[\tilde{x} + \tilde{X}_I(\tilde{t})] \} \\ &\quad - \tilde{R}_I \tilde{J}_Q(\tilde{t}) \{ \delta^{(1)}[\tilde{X}_I(\tilde{t}) - \tilde{x}] - \delta^{(1)}[\tilde{X}_I(\tilde{t}) + \tilde{x}] \} \end{aligned} \quad (4.12)$$

for  $\infty < \tilde{x} < \infty$ . In Appendix B we show that this new diffusion equation forces a temperature jumps at  $\tilde{x} = \pm \tilde{X}_I(\tilde{t})$  and guarantees that the modified Stefan boundary condition, Eq. (3.8), is satisfied.

The temperature profile is given by

$$\begin{aligned} \tilde{T}(\tilde{x}, t) &= \tilde{T}_{\text{Bulk}} + \alpha \int_0^{\tilde{t}} d\tilde{\tau} \frac{e^{-[\tilde{x} - \tilde{X}_I(\tilde{\tau})]^2/4(\tilde{t} - \tilde{\tau})} + e^{-[\tilde{x} + \tilde{X}_I(\tilde{\tau})]^2/4(\tilde{t} - \tilde{\tau})}}{[4\pi(\tilde{t} - \tilde{\tau})]^{1/2}} \dot{\tilde{X}}_I(\tilde{\tau}) \\ &\quad - \tilde{R}_I \int_0^{\tilde{t}} d\tilde{\tau} \frac{e^{-[\tilde{x} - \tilde{X}_I(\tilde{\tau})]^2/4(\tilde{t} - \tilde{\tau})} [\tilde{x} - \tilde{X}_I(\tilde{\tau})] - e^{-[\tilde{x} + \tilde{X}_I(\tilde{\tau})]^2/4(\tilde{t} - \tilde{\tau})} [\tilde{x} + \tilde{X}_I(\tilde{\tau})]}{4\pi^{1/2}(\tilde{t} - \tilde{\tau})^{3/2}} J_Q(\tilde{\tau}), \end{aligned} \quad (4.13)$$

and is coupled to Eq. (3.10) that describes  $\dot{\tilde{X}}_I(\tilde{t})$  and Eq. (3.5) for  $J_Q(\tilde{t})$ . Because  $J_Q(\tilde{t})$  depends on the gradients at the interface, these have to be propagated simultaneously with the temperature at the interface. The details of the numerical solution are described in Appendix B.

Figure 6 displays the dimensionless phase-front velocity and the interfacial temperatures as a function of time for two different supercooling scenarios. The material parameters are the same as above, nonlinear interfacial kinetic is used, but  $\tilde{R}_I = 0.05$ . The velocities are reported as  $\dot{\tilde{X}}_I(\tilde{t})/\beta$ . The cases shown have the following Stephan number  $St = 0.5, 6.1$ . When  $St > 1$ , the long-time steady-state velocity is decreased by the interfacial resistance and the time scale at which the system evolves is longer with interfacial resistance. The final steady-state temperature in the solid is not affected by the interfacial resistance, but a finite temperature jump persists at long times for  $St > 1$ . These conclusions are in perfect

agreement with the long-time asymptotic prediction, also shown on the figure. For  $St < 1$ , the interface velocity tends to zero at long time, albeit slightly more slowly when interfacial resistivities are introduced. For the temperature, we see that a small temperature jump arises at transient times and slowly tends to zero at long times, as predicted by the long-time analysis. In Fig. 7 the full temperature profile for the same supercooling scenarios as in Fig. 6 is shown for selected values of time. A temperature jump is clearly observed for  $St = 6.1$ . There, the jump quickly arises from the uniformly supercooled initial state. It reaches a maximum and eventually decreases slightly to its steady-state value, which agrees with the long-time asymptotic prediction. For the small supercooling scenario,  $St = 0.5$ , the temperature discontinuities remains small at all times and exactly vanishes at long times. This is expected because, in this limit, heat diffusion dominates and washes away any emerging temperature discontinuity. Note

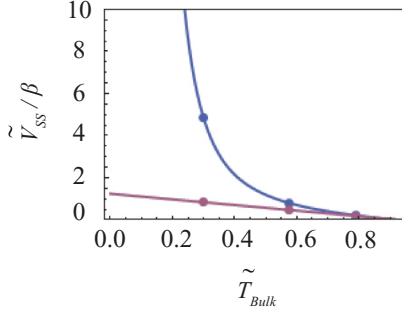


FIG. 5. (Color online) The steady-state interface velocity  $\tilde{V}_{ss}$  is reported as a function of  $\tilde{T}_{Bulk}$  (both  $\tilde{V}_{ss}$  and  $\tilde{T}_{Bulk}$  are dimensionless) for the linear propagating solidification front with nonlinear (top curve, blue) and linear (bottom curve, magenta) interfacial kinetics as predicted by the long-time asymptotic analysis. The points are obtained from the numerical simulation. We have used the materials parameters of SCN. Note that we do not show the range  $0.93 < \tilde{T}_{Bulk} < 1.0$ , where  $\tilde{V}_{ss} = 0$ .

that, relative to the interface position, heat flows from the liquid to the solid. From this observation and Eq. (3.3), we expect the temperature in the solid to be lower than the one in the liquid, in agreement with Fig. 7.

Finally, Fig. 8 shows the dependence on supercooling of the steady-state interfacial velocity with and without an interfacial temperature resistance. As expected, the temperature resistance slows down the solidification process. The steady-state value of the resulting temperature jump is also reported in Fig. 8 as a function of supercooling. These relations directly

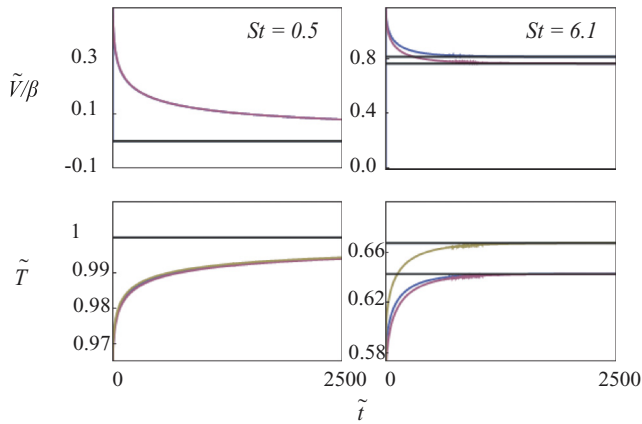


FIG. 6. (Color online) The dimensionless velocity  $\tilde{X}_I(\tilde{t})/\beta$  (top panels) and the dimensionless temperature (bottom panels) of the phase front are shown as a function of dimensionless time with nonlinear interfacial kinetics. For the velocities (top panels), the magenta bottom curve was obtained with a thermal resistivity while the blue top curve was obtained without. Starting from the left, the initial dimensionless temperature is  $\tilde{T}_{Bulk} = 0.965, 0.572645$ . The straight black lines are the long-time steady-state predictions described in Sec. IV B1. For the temperature (bottom panels), the blue curve (second from the bottom) is the interface temperature with no thermal resistivity. The magenta curve (first from the bottom) is the temperature in the solid and the yellow curve (third and last from the bottom) is the temperature in the liquid when there is a thermal resistivity. The straight lines are the long-time steady-state temperature predictions described in Sec. IV B1.

arise from the long-time asymptotic analysis and are in perfect agreement with the case reported in Fig. 6 with  $St = 6.1$  where the interface motion was propagated numerically.

### C. Stability of the planar front

The planar solidification front with constant surface tension has been shown to be unstable for sufficiently long wavelength deformation of the interface. This is the well-known Mullins-Sekerka instability [46,47]. The original stability analysis was performed using a local equilibrium description of the interface [Eq. (2.9)]. Here we show how a Kapitza resistance modifies the Mullins-Sekerka instability.

The analysis starts by considering the following small deformation of the planar interface, which is located at

$$\tilde{x} = \tilde{X}_I(\tilde{t}) + \delta(\tilde{t}) \sin(k\tilde{z}), \quad (4.14)$$

and associated interfacial velocity

$$\tilde{V}_I(\tilde{z}, \tilde{t}) = \dot{\tilde{X}}_I(\tilde{t}) + \dot{\delta}(\tilde{t}) \sin(k\tilde{z}), \quad (4.15)$$

where  $\tilde{z}$  is a direction perpendicular to the interface,  $k$  is the wave number of the deformation, and  $\delta(\tilde{t})$  is a small, time-dependent amplitude. For simplicity, we use linear interfacial kinetics [i.e., Eq. (3.13)] combined with the Gibbs-Thomson boundary condition for the temperature decrease of a curved interface,

$$\frac{\tilde{T}_L(\tilde{X}_I(\tilde{t}) + \delta(\tilde{t}) \sin(k\tilde{z}), \tilde{t}) + \tilde{T}(\tilde{X}_I(\tilde{t}) + \delta(\tilde{t}) \sin(k\tilde{z}), \tilde{t})}{2} = 1 - \Gamma \delta(\tilde{t}) k^2 \sin(k\tilde{z}) - \frac{1}{\beta\gamma} \tilde{V}_I(\tilde{z}, \tilde{t}), \quad (4.16)$$

where all parameters have been defined previously except  $\Gamma$ , which is the surface tension of the interface. Corrections to these profiles due to the deformation of the interface at  $St > 1$  are written as

$$\begin{aligned} \tilde{T}_S(\tilde{x}, \tilde{z}, \tilde{t}) &= \tilde{T}_S^{(0)}(\tilde{x}, \tilde{t}) + \delta(\tilde{t}) \tilde{B}_S \sin(k\tilde{z}) e^{\omega_S(\tilde{x} - \tilde{V}_{ss}\tilde{t})}, \\ \tilde{T}_L(\tilde{x}, \tilde{z}, \tilde{t}) &= \tilde{T}_L^{(0)}(\tilde{x}, \tilde{t}) + \delta(\tilde{t}) \tilde{B}_L \sin(k\tilde{z}) e^{-\omega_L(\tilde{x} - \tilde{V}_{ss}\tilde{t})}, \end{aligned} \quad (4.17)$$

where the steady-state planar interface [ $\delta(\tilde{t}) = 0$ ] temperature profiles,  $\tilde{T}_S^{(0)}$  and  $\tilde{T}_L^{(0)}$ , are given by Eq. (4.9). In this last equation, we introduced the following quantities:

$$\begin{aligned} \omega_S &= \frac{\tilde{V}_{ss}}{2} \left[ 1 + \sqrt{1 + \left(\frac{k}{\tilde{V}}\right)^2} \right], \\ \omega_L &= \frac{\tilde{V}_{ss}}{2} \left[ \sqrt{1 + \left(\frac{k}{\tilde{V}}\right)^2} - 1 \right]. \end{aligned} \quad (4.18)$$

These guarantee that the corrected temperature profile satisfy the diffusion equation [the first two lines of Eq. (3.2)] and that the corrections tend to zero away from the interface. These profiles are inserted in Eq. (4.16), which includes the surface tension effects, and in Eqs. (3.5) and (3.8) for the temperature jump and the conservation of energy. The result is expanded to first order in  $\delta(\tilde{t})$ , and solutions for  $\tilde{B}_S$  and  $\tilde{B}_L$  and  $\delta(\tilde{t})$  are obtained in terms of the steady-state variables  $\tilde{T}_S^I$ ,  $\tilde{T}_L^I$ , and  $\tilde{V}_{SS}$  given in Sec. IV B1 or equivalently, in terms of the material properties. The important point is that  $\delta(\tilde{t})$  is given as

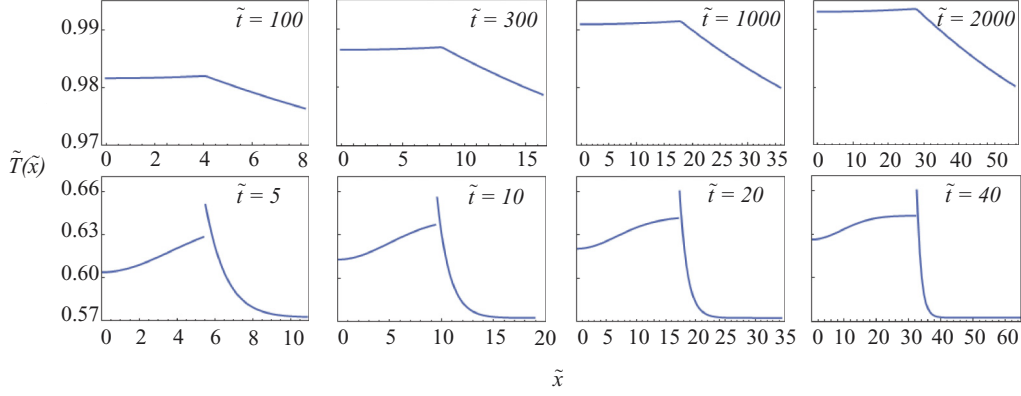


FIG. 7. (Color online) The temperature profile for  $\tilde{T}_{\text{Bulk}} = 0.965$  ( $St = 0.5$ ) (top) and  $\tilde{T}_{\text{Bulk}} = 0.5726$  ( $St = 6.1$ ) (bottom) with  $\tilde{R}_I = 0.05$  (Both  $\tilde{T}$  and  $\tilde{x}$  are dimensionless). From left to right, the temperature profile is shown for four different increasing times written on each panel. Nonlinear interfacial kinetics is used. A temperature jump is observed at all times for  $\tilde{T}_{\text{Bulk}} = 0.5726$ . For  $\tilde{T}_{\text{Bulk}} = 0.965$ , the temperature jump at the interface is smaller than the line thickness.

the solution of the following ordinary differential equation in time:

$$\dot{\delta}(\tilde{t}) = \Lambda \delta(\tilde{t}). \quad (4.19)$$

An exact expression for  $\Lambda$  can be obtained, but it is more instructive to report it in various limits. In all cases we have used the limit  $k \gg \tilde{V}_{ss}$  (which may not be valid for rapid solidification) to compare with Refs. [46,47] which use that approximation. Then we report the result for small and large  $\tilde{R}_I$ ,

$$\Lambda = \begin{cases} \frac{\beta\gamma k(\beta\gamma(1-\alpha-\tilde{T}_{\text{Bulk}})-2\Gamma k^2)}{2k+\beta\gamma\alpha} & \text{when } \tilde{R}_I \rightarrow 0 \\ -\frac{2\beta\gamma\Gamma k^3}{2k+\beta\gamma(2-2\tilde{T}_{\text{Bulk}}-\alpha)} & \text{when } \tilde{R}_I \rightarrow \infty \end{cases}.$$

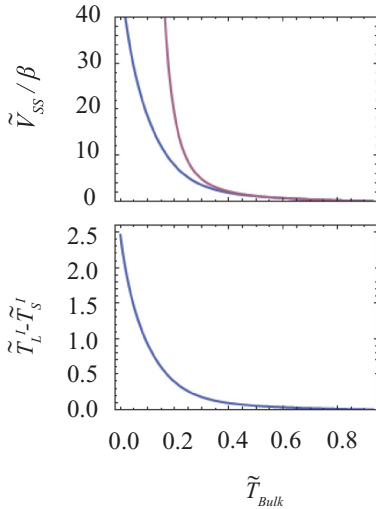


FIG. 8. (Color online) Top panel: The steady-state interface velocity  $\tilde{V}_{ss}$  is reported as a function of  $\tilde{T}_{\text{Bulk}}$  (both  $\tilde{V}_{ss}$  and  $\tilde{T}_{\text{Bulk}}$  are dimensionless) for the propagating solidification with nonlinear kinetics with a thermal resistance of  $\tilde{R}_I = 0.05$  (blue, bottom curve) and no thermal resistance (magenta, top curve) as predicted by the long-time asymptotic analysis. Bottom panel: The dependence of the temperature jump  $\tilde{T}_L - \tilde{T}_S$  on  $\tilde{T}_{\text{Bulk}}$  as predicted by the long-time asymptotics is reported with  $\tilde{R}_I = 0.05$ .

The following conclusions can be drawn. When  $\tilde{R}_I = 0$ , the standard Mullins-Sekerka instability is observed. Any sinusoidal deformation of the interface that has a large wavelength such that  $1/k > [\beta\gamma(1-\alpha-\tilde{T}_{\text{Bulk}})/(2\Gamma)]^{1/2}$  will tend to grow ( $\Lambda$  is positive). Remember that we restrict ourselves to cases where  $St > 1$  and hence  $(1-\alpha-\tilde{T}_{\text{Bulk}}) > 0$ . As the Kapitza resistance increases, that wavelength becomes larger. In other words, the interfacial thermal resistance makes the interface more stable to large wavelength deformation. When  $\tilde{R}_I \rightarrow \infty$ , all deformations are stable, but the  $k = 0$  one ( $\Lambda$  is positive except at  $k = 0$  where it vanishes). Clearly,  $\tilde{R}_I$  will always be finite so the planar interface will always be unstable, but the instability arises at longer wavelengths with a finite  $\tilde{R}_I$ .

## V. DISCUSSION

In this paper we report the effects of nonlinear interfacial kinetics and nonzero Kapitza resistance on the dynamics of the planar front during solidification from an undercooled melt. Our results show that both modifications to the boundary conditions at the interface lead to differences in transient times and steady-state velocities. The nonlinear interfacial kinetics increase the solidification rate while the thermal resistance decreases it. It is in that sense that the two effects compete.

The parameter that establishes whether a traveling wave solution (a planar front advancing with a nonzero steady-state velocity) will be obtained or not at long times is the Stephan number. The newly included interfacial effects do not modify this analysis. Traveling-wave solutions are still obtained when  $St > 1$ . On the other hand, the transient behavior of the phase front is modified by the new interfacial conditions and, when  $St > 1$ , so is the steady-state velocity.

The main results of our work are as follows. For  $St > 1$ , the steady-state temperature in the solid phase is constant and equal to  $\tilde{T}_{\text{Bulk}} + \alpha$ , irrespective of the interfacial dynamics or the Kapitza resistance. The steady-state temperature in the liquid phase decays exponentially away from the interface, but its value close to the interface is larger if  $\tilde{R}_I > 0$ , in which case the steady-state velocity of the front is smaller. Faster dynamics is observed with nonlinear interfacial dynamics and no Kapitza resistance. A stability analysis shows how the

Kapitza resistance shifts the unstable deformation of the planar interface towards larger wavelengths.

The materials parameters of SCN were used in our case study. In this case, the new interfacial boundary conditions showed very little effects when  $St < 1$ . This may not be the case for other materials. In fact, if the argument of the hyperbolic sine in Eqs. (3.9) is larger than one, the transient-time behavior of the front will be highly affected by the nonlinear kinetics, even if  $St < 1$ . On the other hand, in this regime, the final state will always tend to equilibrium at long times (zero phase front velocity and an interface temperature that tends towards  $T_{\text{Melt}}$ ). The same can be said for the interfacial resistance. If its value is large enough. The time scale of the solidification could be significantly reduced even if  $St < 1$ . In this case the system would tend to equilibrium more slowly.

This work is especially relevant to rapid solidification experiments, where the effects discussed are expected to be larger. We are fully aware that the planar front geometry is idealistic (as shown by the Mullins-Sekerka stability analysis). On the other hand, the nonlinear dependence between the steady-state velocity and the supercooled bulk temperature that arises with nonlinear interfacial kinetics should also be observed in a real system in the appropriate regime. Similarly, interfacial resistances will slow down the solidification when they are important, irrespective of the system's geometry. We studied these new effects using the planar geometry because of its simplicity. In the future our goal is to include them in isolated dendritic growth models. There, comparison with rapid solidification experiments will be easier.

Throughout our analysis, we have used equal densities, heat capacities, and thermal diffusivities in the liquid and solid phases. This was done for mathematical simplicity. Nevertheless, for SCN, this turns out to be a decent approximation. Further, we took the material properties to be independent of temperature. We are well aware that this is an oversimplification and that temperature dependence of the densities, heat capacities, and diffusivities probably need to be taken into account in highly supercooled systems. We are not aware of any estimate for the value of the Kapitza resistance of pure substance, the previous measurements of the Kapitza resistance have been for two-component solid-liquid systems [22].

We did not consider any effect of buoyancy driven convection here. In other words, we assumed zero gravity. For rapid solidification experiments carried on earth, buoyancy driven convection necessarily arises. On the other hand, dendritic growth studies show that the convection only plays an important role at small Stephan number, when the solidification is slow. Because this work is primarily interested with rapid solidification, even on earth, buoyancy-driven convection can be neglected.

Using our notation, Fried and Shen [30] claimed that traveling-wave solutions can be found in the limit  $\beta \rightarrow \infty$  when  $\tilde{R}_I \neq 0$ . Understanding that this scenario is hypothetical ( $\beta$  is related to the unidirectional equilibrium constant, which must be finite), this statement can still be misleading. No matter how large  $\beta$  becomes, our work shows that a nonzero steady-state velocity always arises when  $St > 1$  and is given by Eq. (3.10). A nonzero  $\tilde{R}_I$  simply *bounds* the value of the

steady-state velocity, which may be what is meant in Ref. [30]. Physically, this means that when  $\beta$  is very large, an equally large amount of heat will cross the boundary at any given time in the absence of a thermal resistance and  $\tilde{V}_{ss}$  will scale linearly with  $\beta$ . With a finite interfacial resistance, part of the energy that crosses the phase boundary is lost and a maximum velocity is reached at large  $\beta$ .

Finally, we want to make a distinction between our work and the one of Galenko *et al.* [31], which is also relevant to rapid solidification processes. There, the heat transfer is bounded by a finite speed. This results in a nonzero Kapitza resistance at the interface *and* modifies the evolution of the temperature profiles in the bulk (an hyperbolic equation replaces the usual diffusion equation). Our work singles out the interfacial effects. In other words, this means that we are considering systems where the heat transfer is bounded by a large speed in both bulk phases (there, the heat transfer remains diffusive), but a much smaller speed in the region of the interface while Galenko *et al.* assumed that this upperbound for the heat transfer is the same throughout the system. Our method is supported by recent experiment, where temperature jumps are observed at an interface and where the standard diffusion equation holds in the bulk [22].

## ACKNOWLEDGMENTS

We would like to thank the Canadian Space Agency for funding this research. B.P. also thanks the Natural Sciences and Engineering Research Council of Canada for working under their visiting fellow program.

## APPENDIX A: LONG-TIME ASYMPTOTICS

The Charach *et al.* argument starts by rewriting the temperature diffusion equation in a coordinate system where the interface is fixed. This is done with the change of variable  $y = \tilde{x}/\tilde{X}_I(\tilde{t})$ . In these units, the diffusion equation reads

$$\tilde{X}_I(\tilde{t})^2 \frac{\partial \tilde{T}_{S(L)}}{\partial \tilde{t}} = \frac{\partial^2 \tilde{T}_{S(L)}}{\partial y^2} + y \tilde{X}_I(\tilde{t}) \dot{\tilde{X}}_I(\tilde{t}) \frac{\partial \tilde{T}_{S(L)}}{\partial y}, \quad (\text{A1})$$

valid in the solid for  $0 < y < 1$  and in the liquid for  $1 < y < \infty$ . At the system's boundary, the following conditions apply:

$$\left( \frac{\partial \tilde{T}_S(y, \tilde{t})}{\partial y} \right)_{y=0} = 0, \quad \tilde{T}_S(1, \tilde{t}) = \tilde{T}_S^I(\tilde{t}), \quad (\text{A2})$$

$$\tilde{T}_L(1, \tilde{t}) = \tilde{T}_L^I(\tilde{t}), \quad \tilde{T}_L(\infty, \tilde{t}) = \tilde{T}_{\text{Bulk}}.$$

The exact form for  $\tilde{T}_S^I(\tilde{t})$  and  $\tilde{T}_L^I(\tilde{t})$  is left unspecified at this point.

In the solid, the temperature profile postulated in Ref. [28] is

$$\tilde{T}_S(y, \tilde{t}) = A_2(\tilde{t})(y^2 - 1) + \tilde{T}_S^I(\tilde{t}) \quad (\text{A3})$$

and satisfies both solid boundary conditions. Note that Eq. (A1) can only be satisfied approximately with this form of  $\tilde{T}_S$ . On the other hand, Charach *et al.* obtained a differential equation for  $A_2(\tilde{t})$  by integrating Eq. (A1) over the solid domain. The result is

$$\dot{A}_2(\tilde{t}) = \dot{\tilde{T}}_S^I(\tilde{t}) - \left[ \frac{\dot{\tilde{X}}_I(\tilde{t})}{\tilde{X}_I(\tilde{t})} + \frac{3}{\tilde{X}_I(\tilde{t})^2} \right] A_2(\tilde{t}). \quad (\text{A4})$$

For the liquid, Eq. (A1) is further rewritten in terms of the variable  $\mu = (y - 1)\tilde{X}_I(\tilde{t})\dot{\tilde{X}}_I(\tilde{t})$ :

$$\frac{\partial \tilde{T}_L(\mu, \tilde{t})}{\partial \tilde{t}} = \dot{\tilde{X}}_I(\tilde{t})^2 \left\{ \frac{\partial \tilde{T}_L(\mu, \tilde{t})}{\partial \mu^2} + \left[ 1 - \mu \frac{\dot{\tilde{X}}_I(\tilde{t})}{\dot{\tilde{X}}_I(\tilde{t})^3} \right] \frac{\partial \tilde{T}_L(\mu, \tilde{t})}{\partial \mu} \right\}. \quad (\text{A5})$$

The claim is that, at long times, the time dependence of the profile is dominated by  $\mu$  so that the left-hand side of the last equation can be set to zero. Within this approximation, the long-time temperature profile in the liquid is

$$\tilde{T}_L(\mu, \tilde{t}) = \tilde{T}_{\text{Bulk}} + \frac{\tilde{T}_L^I(\tilde{t}) - \tilde{T}_{\text{Bulk}}}{\text{Erfc}[\Omega(\tilde{t})]} \times [1 + g(\tilde{t})(x - 1)\tilde{X}_I(\tilde{t})\dot{\tilde{X}}_I(\tilde{t})], \quad (\text{A6})$$

where  $g(\tilde{t}) = -\dot{\tilde{X}}_I(\tilde{t})/\dot{\tilde{X}}_I(\tilde{t})^3$ ,  $\Omega = [2g(\tilde{t})]^{-1/2}$  and Erfc is the complimentary error function. Charach's argument is based on conservation of energy. There is no heat flux on the boundary at  $\tilde{x} = 0$  and because the other boundary is at infinity, the total energy of the system is conserved so we can write

$$\int_0^{\tilde{X}_I(\tilde{t})} d\tilde{x} [\tilde{T}_S(\tilde{x}, \tilde{t}) - \tilde{T}_{\text{Bulk}}] + \int_{\tilde{X}_I(\tilde{t})}^{\infty} d\tilde{x} [\tilde{T}_S(\tilde{x}, \tilde{t}) - \tilde{T}_{\text{Bulk}}] = \alpha [\tilde{X}_I(\tilde{t}) - 1]. \quad (\text{A7})$$

The approximate profiles in the solid and liquid are inserted in this conservation of energy equation to give

$$-\frac{2}{3}A_2(\tilde{t}) + \tilde{T}_S^I(\tilde{t}) - \tilde{T}_{\text{Bulk}} + \frac{\tilde{T}_L^I(\tilde{t}) - \tilde{T}_{\text{Bulk}}}{g(\tilde{t})\tilde{X}_I(\tilde{t})\dot{\tilde{X}}_I(\tilde{t})} [W(\Omega(\tilde{t})) - 1] = \alpha [1 - \tilde{X}_I(\tilde{t})^{-1}], \quad (\text{A8})$$

where  $W(\Omega(\tilde{t})) = \pi^{1/2}\Omega e^{\Omega^2}\text{Erfc}(\Omega)$ . We now follow Charach's method and show how asymptotic expressions for  $\tilde{X}_I(\tilde{t})$ ,  $\dot{\tilde{X}}_I(\tilde{t})$ ,  $\tilde{T}_S^I(\tilde{t})$ , and  $\tilde{T}_L^I(\tilde{t})$  are obtained at long times. The only difference here versus the work done in Ref. [28] is that we allow for nonlinear interfacial kinetics and a temperature discontinuity.

### 1. Traveling wave solutions, $\text{St} > 1$

We assume that the long-time interface position follows

$$\tilde{X}_I(\tilde{t}) = \tilde{V}_{SS}\tilde{t}^\eta, \quad (\text{A9})$$

with  $1/2 < \eta \leq 1$ . Other cases will come next. Here,  $g(\tilde{t}) = (1 - \eta)\eta^{-2}\tilde{V}_{SS}^{-2}\tilde{t}^{1-2\eta}$ , and hence,  $g(\tilde{t}) \rightarrow 0$  and  $\Omega(\tilde{t}) \rightarrow \infty$  when  $\tilde{t} \rightarrow \infty$  unless  $\eta = 1$ . Using asymptotic expressions for the complementary error function, the long-time temperature profile in the liquid is now written as

$$\tilde{T}_L(y, \tilde{t}) = \tilde{T}_{\text{Bulk}} + [\tilde{T}_L^I(\tilde{t}) - \tilde{T}_{\text{Bulk}}] \times \exp[-(y - 1)\tilde{X}_I(\tilde{t})\dot{\tilde{X}}_I(\tilde{t}) - (y - 1)^2g(\tilde{t})\tilde{X}_I(\tilde{t})^2\dot{\tilde{X}}_I(\tilde{t})^2]. \quad (\text{A10})$$

Further, when  $\eta = 1$ , we get the so-called traveling wave solution, and the second term in the exponential vanishes:

$$\tilde{T}_L(y, \tilde{t}) = \tilde{T}_{\text{Bulk}} + [\tilde{T}_L^I(\tilde{t}) - \tilde{T}_{\text{Bulk}}] \exp[-(y - 1)\tilde{V}_{SS}\tilde{t}]. \quad (\text{A11})$$

Taking  $\eta = 1$  henceforth, we examine what it predicts for the steady-state velocity,  $\tilde{V}_{SS}$ , the interfacial temperatures, and assess its range of validity. The long-time expression for the temperature jump gives

$$\tilde{T}_L^I(\tilde{t}) - \tilde{T}_S^I(\tilde{t}) = -R_I \left[ -\tilde{V}_{SS}\tilde{T}_S^I(\tilde{t}) - \frac{2A_2(\tilde{t})}{\tilde{V}_{SS}\tilde{t}} \right]. \quad (\text{A12})$$

The fact that the last term on the right-hand side vanishes at long times, combined with a kinetic expression of the form  $\tilde{V}_{SS} = F(\tilde{T}_L^I(\tilde{t}), \tilde{T}_S^I(\tilde{t}))$ , linear or not, shows that any of the interface temperatures is a function of  $\tilde{V}_{SS}$  only. Hence, Eq. (A4) becomes

$$\dot{A}_2(\tilde{t}) = -\frac{1}{\tilde{t}}A_2(\tilde{t}) \quad (\text{A13})$$

and  $A_2(\tilde{t}) = A/\tilde{t}$  with  $A$  a constant. At long times, the temperature profile in the solid is

$$\tilde{T}_S(y, \tilde{t}) = \tilde{T}_S^I(\tilde{t}). \quad (\text{A14})$$

The long-time limit of Eq. (A8) simplifies to

$$\tilde{T}_S^I(\tilde{t}) = \alpha + \tilde{T}_{\text{Bulk}}, \quad (\text{A15})$$

and hence,

$$\tilde{T}_L^I(\tilde{t}) = (1 + R_I\tilde{V}_{SS})(\alpha + \tilde{T}_{\text{Bulk}}). \quad (\text{A16})$$

Hence, the steady-state velocity is obtained by solving this last expression simultaneously with the interfacial kinetics expression. In the main text, we discuss how these last equations imply that traveling-wave solutions are obtained when  $\text{St} > 1$ .

### 2. $\text{St} < 1$

Here, we consider the case where  $\tilde{X}_I(\tilde{t}) = c\tilde{t}^{1/2}$  and show that it gives a solution for  $\text{St} < 1$ . First, the temperature jump expression now becomes

$$\tilde{T}_L^I(\tilde{t}) - \tilde{T}_S^I(\tilde{t}) = R_I\tilde{t}^{-1/2} \left[ \frac{c}{2}\tilde{T}_S^I(\tilde{t}) - \frac{2}{c}A_2(\tilde{t}) \right]. \quad (\text{A17})$$

Combining this with

$$A_2(\tilde{t}) = -\tilde{t}^{-1} \frac{c}{4} \frac{\partial \tilde{T}_S^I(\tilde{t})}{\partial \dot{\tilde{X}}_I(\tilde{t})} - \tilde{t}^{-1} \frac{c^2 + 6}{2c^2} A_2(\tilde{t}), \quad (\text{A18})$$

and assuming that the derivative on the first term of the right-hand side of the last equation is nonzero for small  $\dot{\tilde{X}}_I(\tilde{t})$ , we obtain that  $\tilde{T}_L^I(\tilde{t}) = \tilde{T}_S^I(\tilde{t}) = 1$  and  $A_2(\tilde{t}) \propto \tilde{t}^{-1/2}$  at long times.

In this case, Eq. (A8) simplifies to

$$\text{St} = \pi^{1/2} \frac{c}{2} e^{c^2/4} \text{Erfc}(c/2), \quad (\text{A19})$$

where we used  $\text{St} = (1 - \tilde{T}_{\text{Bulk}})/\alpha$ . The right-hand side of that equation lies between 0 and 1 for all  $c$ . Hence, a long-time solution of the type  $\tilde{X}_I(\tilde{t}) = c\tilde{t}^{1/2}$  is obtained when  $\text{St} < 1$ .

## APPENDIX B: DISCRETIZING THE INTEGRAL

The temperature profile at all times is given by

$$\begin{aligned} \tilde{T}(\tilde{x}, t) = & \tilde{T}_{\text{Bulk}} + \alpha \int_0^{\tilde{t}} d\tilde{\tau} \frac{e^{-[\tilde{x} - \tilde{X}_I(\tilde{\tau})]^2/4(\tilde{t} - \tilde{\tau})} + e^{-[\tilde{x} + \tilde{X}_I(\tilde{\tau})]^2/4(\tilde{t} - \tilde{\tau})}}{[4\pi(\tilde{t} - \tilde{\tau})]^{1/2}} \dot{\tilde{X}}_I(\tilde{\tau}) \\ & - R_I \int_0^{\tilde{t}} d\tilde{\tau} \frac{e^{-[\tilde{x} - \tilde{X}_I(\tilde{\tau})]^2/4(\tilde{t} - \tilde{\tau})} [\tilde{x} - \tilde{X}_I(\tilde{\tau})] - e^{-[\tilde{x} + \tilde{X}_I(\tilde{\tau})]^2/4(\tilde{t} - \tilde{\tau})} [\tilde{x} + \tilde{X}_I(\tilde{\tau})]}{4\pi^{1/2}(\tilde{t} - \tilde{\tau})^{3/2}} J_Q(\tilde{\tau}). \end{aligned} \quad (\text{B1})$$

We now show how these integrals are performed numerically. When there are no temperature jumps, the second term on the right-hand side is omitted. We assume that  $\dot{\tilde{X}}_I(\tilde{\tau})$  and  $J_Q(\tilde{\tau})$  are constant over a short time interval  $\Delta\tilde{t}$ . When this is done, the time integral is partitioned into  $N$  segments, and the temperate profile is written as

$$\tilde{T}(\tilde{x}, t) - \tilde{T}_{\text{Bulk}} = \sum_{n=0}^{N-1} \left\{ \alpha \dot{\tilde{X}}_I(n\Delta\tilde{t}) [I_{1,n}^A(x) + I_{1,n}^B(x)] - R_I J_Q(n\Delta\tilde{t}) [I_{2,n}^A(x) - I_{2,n}^B(x)] \right\}, \quad (\text{B2})$$

where  $N\Delta\tilde{t} = \tilde{t}$  and where

$$I_{1,n}^A = \int_{(N-n-1)\Delta\tilde{t}}^{(N-n)\Delta\tilde{t}} du \frac{\exp\{-[S_n(x) + u\dot{\tilde{X}}_I(n\Delta\tilde{t})]^2/4u\}}{(4\pi u)^{1/2}}, \quad (\text{B3a})$$

$$I_{1,n}^B = \int_{(N-n-1)\Delta\tilde{t}}^{(N-n)\Delta\tilde{t}} du \frac{\exp\{-[Z_n(x) + u\dot{\tilde{X}}_I(n\Delta\tilde{t})]^2/4u\}}{(4\pi u)^{1/2}}, \quad (\text{B3b})$$

$$I_{2,n}^A = \int_{(N-n-1)\Delta\tilde{t}}^{(N-n)\Delta\tilde{t}} du \frac{\exp\{-[S_n(x) + u\dot{\tilde{X}}_I(n\Delta\tilde{t})]^2/4u\}}{4\pi^{1/2}u^{3/2}} [S_n(x) + u\dot{\tilde{X}}_I(n\Delta\tilde{t})] = -\frac{\partial I_{1,n}^A}{\partial S_n(x)}, \quad (\text{B3c})$$

$$I_{2,n}^B = \int_{(N-n-1)\Delta\tilde{t}}^{(N-n)\Delta\tilde{t}} du \frac{\exp\{-[Z_n(x) - u\dot{\tilde{X}}_I(n\Delta\tilde{t})]^2/4u\}}{4\pi^{1/2}u^{3/2}} [Z_n(x) - u\dot{\tilde{X}}_I(n\Delta\tilde{t})] = -\frac{\partial I_{1,n}^B}{\partial Z_n(x)}, \quad (\text{B3d})$$

where we introduced the following functions:

$$S_n(x) = x - \tilde{X}_I(n\Delta\tilde{t}) - (N-n)\Delta\tilde{t}\dot{\tilde{X}}_I(n\Delta\tilde{t}) \quad (\text{B4a})$$

and

$$Z_n(x) = x + \tilde{X}_I(n\Delta\tilde{t}) + (N-n)\Delta\tilde{t}\dot{\tilde{X}}_I(n\Delta\tilde{t}). \quad (\text{B4b})$$

The interfacial kinetics is described in terms of temperature at the interface. Hence, we let  $x \rightarrow \tilde{X}_I(N\Delta\tilde{t})$  in the last equations. At this position, one can show that  $S_n \leq 0$  (the equality is for  $n = N - 1$ ) and  $Z_n > 0$ . The integration is performed and  $I_{1,n}^A$  and  $I_{1,n}^B$  are rewritten:

$$\begin{aligned} I_{1,n}^A = & \frac{1}{2\dot{\tilde{X}}_I(n\Delta\tilde{t})} \left( e^{-S_n\dot{\tilde{X}}_I(n\Delta\tilde{t})} \left[ \text{Erf} \left( \frac{S_n - (N-n-1)\Delta\tilde{t}\dot{\tilde{X}}_I(n\Delta\tilde{t})}{2((N-n-1)\Delta\tilde{t})^{1/2}} \right) - \text{Erf} \left( \frac{S_n - (N-n)\Delta\tilde{t}\dot{\tilde{X}}_I(n\Delta\tilde{t})}{2((N-n)\Delta\tilde{t})^{1/2}} \right) \right] \right. \\ & \left. + \text{Erf} \left( \frac{S_n + (N-n)\Delta\tilde{t}\dot{\tilde{X}}_I(n\Delta\tilde{t})}{2((N-n)\Delta\tilde{t})^{1/2}} \right) - \text{Erf} \left( \frac{S_n + (N-n-1)\Delta\tilde{t}\dot{\tilde{X}}_I(n\Delta\tilde{t})}{2((N-n-1)\Delta\tilde{t})^{1/2}} \right) \right), \end{aligned} \quad (\text{B5})$$

$$\begin{aligned} I_{1,n}^B = & \frac{1}{2\dot{\tilde{X}}_I(n\Delta\tilde{t})} \left( e^{Z_n\dot{\tilde{X}}_I(n\Delta\tilde{t})} \left[ \text{Erf} \left( \frac{Z_n + (N-n)\Delta\tilde{t}\dot{\tilde{X}}_I(n\Delta\tilde{t})}{2((N-n)\Delta\tilde{t})^{1/2}} \right) - \text{Erf} \left( \frac{Z_n + (N-n-1)\Delta\tilde{t}\dot{\tilde{X}}_I(n\Delta\tilde{t})}{2((N-n-1)\Delta\tilde{t})^{1/2}} \right) \right] \right. \\ & \left. + \text{Erf} \left( \frac{Z_n - (N-n-1)\Delta\tilde{t}\dot{\tilde{X}}_I(n\Delta\tilde{t})}{2((N-n-1)\Delta\tilde{t})^{1/2}} \right) - \text{Erf} \left( \frac{Z_n - (N-n)\Delta\tilde{t}\dot{\tilde{X}}_I(n\Delta\tilde{t})}{2((N-n)\Delta\tilde{t})^{1/2}} \right) \right). \end{aligned} \quad (\text{B6})$$

Note that the limit  $n \rightarrow N - 1$  is well defined in both cases.  $I_{2,n}^A$  and  $I_{2,n}^B$  can now be rewritten as follows:

$$I_{2,n}^A = \frac{1}{2} e^{-S_n\dot{\tilde{X}}_I(n\Delta\tilde{t})} \left[ \text{Erf} \left( \frac{S_n - (N-n-1)\Delta\tilde{t}\dot{\tilde{X}}_I(n\Delta\tilde{t})}{2((N-n-1)\Delta\tilde{t})^{1/2}} \right) - \text{Erf} \left( \frac{S_n - (N-n)\Delta\tilde{t}\dot{\tilde{X}}_I(n\Delta\tilde{t})}{2((N-n)\Delta\tilde{t})^{1/2}} \right) \right], \quad (\text{B7})$$

valid for  $n < N - 1$  and

$$I_{2,n}^B = \frac{1}{2} e^{Z_n \dot{\tilde{X}}_I(n\Delta\tilde{t})} \left[ \text{Erf} \left( \frac{Z_n + (N - n - 1)\Delta\tilde{t} \dot{\tilde{X}}_I(n\Delta\tilde{t})}{2((N - n - 1)\Delta\tilde{t})^{1/2}} \right) - \text{Erf} \left( \frac{Z_n + (N - n)\Delta\tilde{t} \dot{\tilde{X}}_I(n\Delta\tilde{t})}{2((N - n)\Delta\tilde{t})^{1/2}} \right) \right], \quad (\text{B8})$$

valid for all  $n$ . When  $n = N - 1$ ,  $I_{2,n}^A$  gives a different answer if the limit  $\tilde{x} \rightarrow \tilde{X}_I(N\Delta\tilde{t})$  is taken from the liquid side ( $\tilde{x} \rightarrow \tilde{X}_I(N\Delta\tilde{t})^+$ ) or from the solid side ( $\tilde{x} \rightarrow \tilde{X}_I(N\Delta\tilde{t})^-$ ) because  $S_n$  changes sign. The results are

$$I_{2,N-1}^A(\text{liquid}) = \frac{1}{2} \left( 1 + \text{Erf} \left( \frac{\Delta\tilde{t}^{1/2} \dot{\tilde{X}}_I((N - 1))}{2} \right) \right) \quad (\text{B9})$$

and

$$I_{2,N-1}^A(\text{solid}) = \frac{1}{2} \left( -1 + \text{Erf} \left( \frac{\Delta\tilde{t}^{1/2} \dot{\tilde{X}}_I((N - 1))}{2} \right) \right), \quad (\text{B10})$$

which enforces that  $T_L^I - T_S^I = -R_I J_Q(N\Delta\tilde{t})$ .

Because  $J_Q(n\Delta\tilde{t})$  depends on the interface velocity, the interface temperature, and the interface temperature gradients, the latter have to be propagated as well. Using the same procedure, the temperature gradients anywhere in the system can be written as

$$\nabla \tilde{T}(\tilde{x}, t) = \sum_{n=0}^{N-1} \left\{ -\alpha \dot{\tilde{X}}_I(n\Delta\tilde{t}) [I_{2,n}^A(x) + I_{2,n}^B(x)] - R_I J_Q(n\Delta\tilde{t}) [I_{3,n}^A(x) - I_{3,n}^B(x)] \right\}, \quad (\text{B11})$$

where  $I_{2,n}^A$  and  $I_{2,n}^B$  are defined above and where

$$I_{3,n}^A(x) = -\frac{\partial^2 I_{1,n}^A}{\partial S_n(x)^2} \quad (\text{B12})$$

and

$$I_{3,n}^B(x) = -\frac{\partial^2 I_{1,n}^B}{\partial Z_n(x)^2}. \quad (\text{B13})$$

When we set,  $x \rightarrow \tilde{X}_I(N\Delta\tilde{t})$ , the expressions we derived above for  $I_{2,n}^A$  and  $I_{2,n}^B$  are unchanged. For  $I_{3,n}^A$  and  $I_{3,n}^B$ , one has to be more careful. Because these terms arise from the derivative of temperature in the vicinity of a temperature jump, the gradient exactly at  $x = \tilde{X}_I(N\Delta\tilde{t})$  diverges. What we need is the gradient in the solid and liquid close to the interface, so these divergences are dropped. We obtain

$$I_{3,n}^A = \frac{\dot{\tilde{X}}_I(n\Delta\tilde{t})}{2} e^{-S_n \dot{\tilde{X}}_I(n\Delta\tilde{t})} \left[ \text{Erf} \left( \frac{S_n - (N - n)\Delta\tilde{t} \dot{\tilde{X}}_I(n\Delta\tilde{t})}{2((N - n)\Delta\tilde{t})^{1/2}} \right) - \text{Erf} \left( \frac{S_n - (N - n - 1)\Delta\tilde{t} \dot{\tilde{X}}_I(n\Delta\tilde{t})}{2((N - n - 1)\Delta\tilde{t})^{1/2}} \right) \right], \quad (\text{B14})$$

for  $n \leq N - 1$  and

$$I_{3,n}^B = \frac{\dot{\tilde{X}}_I(n\Delta\tilde{t})}{2} e^{-Z_n \dot{\tilde{X}}_I(n\Delta\tilde{t})} \left[ \text{Erf} \left( \frac{Z_n - (N - n)\Delta\tilde{t} \dot{\tilde{X}}_I(n\Delta\tilde{t})}{2((N - n)\Delta\tilde{t})^{1/2}} \right) - \text{Erf} \left( \frac{Z_n - (N - n - 1)\Delta\tilde{t} \dot{\tilde{X}}_I(n\Delta\tilde{t})}{2((N - n - 1)\Delta\tilde{t})^{1/2}} \right) \right], \quad (\text{B15})$$

valid for all  $n$ . Similar to  $I_{2,N-1}^A$ ,  $I_{3,N}^A$  behaves differently if  $x \rightarrow \tilde{X}_I(N\Delta\tilde{t})^\pm$ . The result is

$$I_{3,N-1}^A(\text{liquid}) = -\frac{\dot{\tilde{X}}_I((N - 1)\Delta\tilde{t})}{2} \left( 1 + \text{Erf} \left( \frac{\Delta\tilde{t}^{1/2} \dot{\tilde{X}}_I((N - 1))}{2} \right) \right) \quad (\text{B16})$$

and

$$I_{3,N-1}^A(\text{solid}) = -\frac{\dot{\tilde{X}}_I((N - 1)\Delta\tilde{t})}{2} \left( -1 + \text{Erf} \left( \frac{\Delta\tilde{t}^{1/2} \dot{\tilde{X}}_I((N - 1))}{2} \right) \right). \quad (\text{B17})$$

Hence, these terms also contribute to the discontinuity in the temperature gradient at the interface. From the expression for  $I_{2,N-1}^A$  and  $I_{3,N-1}^B$ , we see that the Stephan boundary condition with a temperature jump, Eq. (3.8), is recovered.

The following iterative procedure is implemented to simulate the propagation front:

(1) At  $\tilde{t} = 0$ , the interfacial temperature is  $\tilde{T}_{\text{Bulk}}$  and all temperature gradients vanish.  $\dot{\tilde{X}}_I(0)$  is obtained from Eq. (3.10) with  $\tilde{T}_S^I = \tilde{T}_L^I = \tilde{T}_{\text{Bulk}}$ .

(2) From  $\dot{\tilde{X}}_I(0)$  and the vanishing temperature gradients,  $\tilde{J}_Q(0)$  is calculated using Eq. (3.5).

(3) Time is changed to  $\tilde{t} = \Delta\tilde{t}$  and the interface position is changed to  $\tilde{X}_I(\Delta\tilde{t}) = \tilde{X}_I(0) + \Delta\tilde{t} \dot{\tilde{X}}_I(0)$  where  $\Delta\tilde{t}$  is small.

(4) Equations (B2) and (B11) with  $N = 1$  are used to get the temperature and temperature gradients for all  $\tilde{x}$  at  $\tilde{t} = \Delta\tilde{t}$ , including at  $\tilde{x} = \tilde{X}_I^\pm(\Delta\tilde{t})$  ( $\pm$  means that we are either on the liquid or solid side of the interface, respectively).

(5) The new interfacial temperatures and temperature gradients are used to get  $\tilde{X}_I(\Delta\tilde{t})$  and  $\tilde{J}_Q(\Delta\tilde{t})$  at  $\tilde{t} = \Delta\tilde{t}$ .

(6) Steps 3, 4, and 5 are repeated for  $\tilde{t} = \Delta\tilde{t}, \dots, M\Delta\tilde{t}$  where the predetermined final time is  $\tilde{t}_{\text{Final}} = M\Delta\tilde{t}$ .

If  $\tilde{R}_I = 0$ , neither the temperature gradients nor  $\tilde{J}_Q$  need to be calculated.

- 
- [1] P. Pelcé, *Dynamics of Curved Fronts* (Academic Press, San Diego, 1988).
- [2] H. M. Singer and J. H. Bilgram, *Europhys. Lett.* **68**, 240 (2004).
- [3] G. P. Ivantsov, *Dokl. Akad. Nauk SSSR* **58**, 567 (1947).
- [4] D. E. Temkin, *Dokl. Akad. Nauk SSSR* **132**, 1307 (1960).
- [5] M. E. Glicksman, E. Winsa, R. C. Hahn, T. A. Lograsso, S. H. Tirmizi, and M. E. Selleck, *Metall. Trans. A* **19**, 1945 (1988).
- [6] M. E. Glicksman, M. B. Koss, L. T. Bushnell, J. C. La-Combe, and E. A. Winsa, *Adv. Space Res.* **16**, 181 (1995).
- [7] M. E. Glicksman, M. B. Koss, and E. A. Winsa, *JOM* **47**, 49 (1995).
- [8] M. E. Glicksman, M. B. Koss, L. T. Bushnell, J. C. La-Combe, and E. A. Winsa, *ISIJ Int.* **35**, 604 (1995).
- [9] R. Ananth and W. N. Gill, *J. Cryst. Growth* **91**, 587 (1988).
- [10] D. Canright and S. H. Davis, *J. Cryst. Growth* **114**, 153 (1991).
- [11] J. S. Langer and H. Müller-Krumbhaar, *J. Cryst. Growth* **42**, 11 (1977).
- [12] J. S. Langer, *Science* **243**, 1150 (1989).
- [13] E. A. Brener and V. I. Melnikov, *Adv. Phys.* **40**, 53 (1991).
- [14] J. J. Hoyt, Mark Asta, and Alain Karma, *Mat. Sci. Eng. R* **41**, 121 (2003).
- [15] P. Zhao, J. C. Heinrich, and D. R. Poirier, *Int. J. Numer. Meth. Eng.* **71**, 25 (2007).
- [16] G. L. Pollack, *Rev. Mod. Phys.* **41**, 48 (1969).
- [17] E. T. Swartz and R. O. Pohl, *Rev. Mod. Phys.* **61**, 605 (1989).
- [18] J.-L. Barrat and F. Chiarutini, *Mol. Phys.* **101**, 1605 (2003).
- [19] H. Ghasemi and C. A. Ward, *Phys. Rev. Lett.* **105**, 136102 (2010).
- [20] F. Duan and C. A. Ward, *Phys. Rev. E* **72**, 056302 (2005).
- [21] F. Duan and C. A. Ward, *Phys. Rev. E* **72**, 056304 (2005).
- [22] H. Ghasemi and C. A. Ward, *J. Phys. Chem. C* **115**, 21311 (2011).
- [23] G. X. Wang and V. Prasad, *Microscale Therm. A* **1**, 143 (1997).
- [24] C. A. Ward, R. D. Findlay, and M. Rizk, *J. Chem. Phys.* **76**, 5599 (1982).
- [25] M. Dejmek and C. A. Ward, *J. Chem. Phys.* **108**, 8698 (1998).
- [26] J. A. W. Elliott and C. A. Ward, *J. Chem. Phys.* **106**, 5667 (1997).
- [27] C. A. Ward and G. Fang, *Phys. Rev. E* **59**, 429 (1999).
- [28] Ch. Charach and B. Zaltzman, *Phys. Rev. E* **47**, 1230 (1993).
- [29] Ch. Charach and B. Zaltzman, *Phys. Rev. E* **47**, 4322 (1994).
- [30] E. Fried and A. Q. Shen, *Continuum Mech. Thermodyn.* **11**, 277 (1999).
- [31] P. K. Galenko and D. A. Danilov, *Phys. Lett. A* **278**, 129 (2000).
- [32] H. S. Carslaw and J. C. Jaeger, *Conduction of Heat in Solids, 2nd ed.* (Oxford University Press, New York, 1959).
- [33] S. T. Huxtable, D. G. Cahill, S. Shenogin, L. Xue, R. Ozisik, P. Barone, M. Usrey, M. S. Stran, G. Siddons, M. Shim, and P. Keblinski, *Nat. Mater.* **2**, 731 (2003).
- [34] J. A. Elliott and C. A. Ward, *Stud. Surf. Sci. Catal.* **104**, 285 (1997).
- [35] J. A. W. Elliott, *Chem. Eng. Ed.* **35**, 274 (2001).
- [36] F. Duan, *J. Phys. D* **42**, 102004 (2009).
- [37] F. Duan, I. Thompson, and C. A. Ward, *J. Phys. Chem. B* **112**, 71 (2008).
- [38] A. H. Persad and C. A. Ward, *J. Phys. B* **114**, 6107 (2010).
- [39] C. A. Wulff and E. F. Westrum, Jr., *J. Phys. Chem.* **67**, 2376 (1963).
- [40] L. Onsager, *Phys. Rev.* **37**, 405 (1931).
- [41] S. Balibar, H. Alles and Alexander. Y. Parshin, *Rev. Mod. Phys.* **77**, 317 (2005).
- [42] J. W. A. Elliott, H. Y. Elmoazzen, and L. E. McGann, *J. Chem. Phys.* **113**, 6573 (2000).
- [43] M. Marder, *Phys. Rev. A* **45**, R2158 (1992).
- [44] H. Löwen, J. Bechhoefer, and L. S. Tuckerman, *Phys. Rev. A* **45**, 2399 (1992).
- [45] M. B. Koss, J. C. Lacombe, L. A. Tennenhouse, M. E. Glicksman, and E. A. Winsa, *Metall. Mater. Trans. A* **30**, 3177 (1999).
- [46] W. W. Mullins and R. F. Sekerka, *J. Appl. Phys.* **35**, 444 (1964).
- [47] J. S. Langer, *Rev. Mod. Phys.* **52**, 1 (1980).